Cantor set structures in the singularities of classical potential scattering

1987 J. Phys. A: Math. Gen. 20 3607

(http://iopscience.iop.org/0305-4470/20/12/015)

J. Phys. A: Math. Gen. **20** (1987) 3607-3617. Printed in the UK

Cantor set structures in the singularities of classical potential scattering

C Jung and H J Scholz

Fachbereich Physik, Universität Bremen, 2800 Bremen, West Germany

Received 31 October 1986

Abstract. A classical mechanical system is analysed which exhibits complicated scattering behaviour. In the set of all incoming asymptotes there is a fractal subset on which the scattering angle is singular. Though in the complement of this Cantor set the deflection function is regular, one can choose impact parameter intervals leading to arbitrarily complicated trajectories. We show how the complicated scattering behaviour is caused by unstable periodic orbits having homoclinic and heteroclinic connections. Thereby a hyperbolic invariant set is created leading to horseshoe chaos in the flow. This invariant set contains infinitely many unstable localised orbits (periodic and aperiodic ones). The stable manifolds of these orbits reach out into the asymptotic region and create the singularities of the scattering function.

1. Introduction

In a typical scattering event a free particle comes in from infinity, enters the potential region and moves in the potential for a finite time. After a while it leaves the potential region and goes off to infinity again as a free particle. Complicated motion can occur inside the potential region for a finite time only and the motion in the asymptotic region is always trivial. Accordingly any typical scattering trajectory is never chaotic, because chaoticity implies complicated motion for ever. This argument may lead to the erroneous conclusion that scattering systems never show chaotic behaviour and that any scattering motion is integrable.

On the other hand, there are a few observations of complicated (chaotic?) behaviour of the outgoing scattering asymptote as a function of the initial conditions. Such behaviour has been reported in vortex scattering in fluid dynamics (Eckhardt and Aref 1987), in classical models of inelastic molecular scattering (Gottdiener 1975, Noid *et al* 1986), in satellite encounters (Petit and Henon 1986) and in classical potential scattering (Eckhardt and Jung 1986). In all these examples a one-dimensional subset of initial conditions has been scanned and some property of the final state, plotted as a function of the initial state, shows singularities on a whole Cantor set.

The occurrence of singularities in the scattering angle is well known from orbiting in rotationally symmetric potentials (Newton 1982, § 5.4). For each energy in an appropriate interval there exists an impact parameter such that the incoming scattering trajectory spirals towards an unstable circular orbit and remains there forever. For this particular combination of energy and impact parameter the scattering trajectory starts on the stable manifold of the periodic orbit. Accordingly for these initial conditions the scattering angle is undefined (singular). However, this singularity alone does not yet indicate complicated behaviour. For rotationally symmetric potentials

0305-4470/87/123607+11$02.50

the angular momentum is a further conserved quantity, whose existence implies integrability of the problem.

We propose to call a scattering motion complicated (or even chaotic) only if there is a fractal set of singularities. In order to obtain a Cantor set of singularities, created by a similar mechanism as in orbiting, there must be an uncountable number of unstable localised orbits which have influence on the asymptotic region.

How such a situation can occur has been shown by Churchill *et al* (1979). These authors prove that the interplay of several unstable periodic orbits can create horseshoe chaos in the Hamiltonian flow on non-compact energy surfaces also, i.e. for unbounded motion. As an example for demonstration they use the Henon-Heiles potential (Henon and Heiles 1964), which is not a proper scattering problem because the potential does not go to 0 if the distance goes to ∞. However, their arguments only use the properties of the interior part of the potential. Therefore their reasoning can be transferred verbatim to any proper scattering potential whose interior part looks similar to the interior part of the Henon-Heiles potential. We shall use such a system to show in a detailed study how the Cantor set of scattering singularities is created by the heteroclinic and homoclinic connections of certain unstable periodic orbits.

Section 2 presents the Cantor set structure of the singularities of the scattering angle as a function of the impact parameter. It gives the plots of several interesting scattering trajectories in position space. From these plots the importance of periodic orbits becomes evident.

In § 3 the periodic orbits which create the complicated scattering behaviour are identified. We show their stable and unstable manifolds in a Poincaré section and show some of their homoclinic and heteroclinic points. In addition we present plots of the orbits belonging to some distinguished points in the Poincaré section.

Section 4 gives a global survey of the singularities of the scattering angle in the space of all initial conditions and § 5 contains conclusions and final remarks.

2. Singularities in the deflection function

In order to keep things as simple as possible and to be able to show plots of trajectories in position space and Poincaré sections we choose a system with two degrees of freedom. The two position space coordinates are x and y, and the canonically conjugate momenta are p_x and p_y. For the Hamiltonian function we take

$$H = p_x^2/2 + p_y^2/2 + \exp[-(x-1/\sqrt{2})^2 - (y-\sqrt{\tfrac{3}{2}})^2] + \exp[-(x-1/\sqrt{2})^2 - (y+\sqrt{\tfrac{3}{2}})^2] + \exp[-(x+\sqrt{2})^2 - y^2]. \quad (1)$$

Figure 1 gives some contour lines and the critical points of the potential. The system is invariant under rotations by $\pm\frac{2}{3}\pi$. The potential has seven critical points: one relative minimum in $P_0 = (0, 0)$ at energy $E_0 = 0.40\ldots$; three saddle points P_{s1}, P_{s2}, P_{s3} at energy $E_s = 0.45\ldots$, $P_{s1} = (0.6\ldots, 0)$. The coordinates of P_{s2} and P_{s3} are obtained by rotating P_{s1} around $\pm\frac{2}{3}\pi$, and three maxima P_{M1}, P_{M2}, P_{M3} at energy $E_M = 1.005\ldots$, $P_{M1} = (-1.4\ldots, 0)$. The coordinates of P_{M2} and P_{M3} are obtained by rotating P_{M1} around $\pm\frac{2}{3}\pi$.

The straight line asymptotes of the system are labelled by the three quantities E, α, b. E is the energy in the asymptotic region, $E = (p_x^2 + p_y^2)/2$. α is the direction of the momentum, $\alpha = \tan^{-1}(p_y/p_x)$. b is the impact parameter, $b = (xp_y - yp_x)/(p_x^2 + p_y^2)^{1/2}$. In the following we denote by $\mathcal{A}$ the three-dimensional $E/\alpha/b$

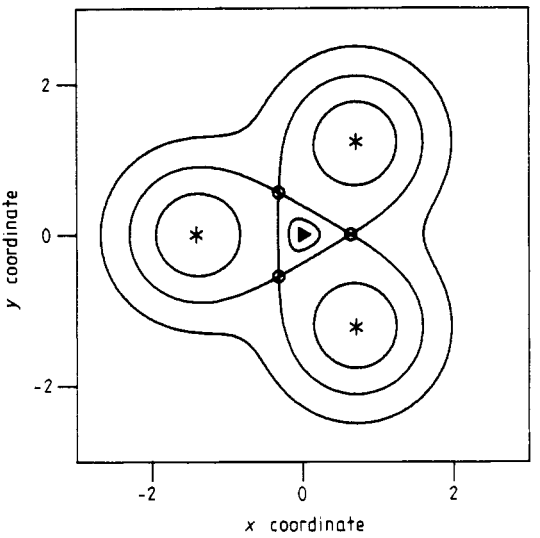

Figure 1. Some contour lines and the critical points of the potential of equation (1). ► is a relative minimum, ○ are three saddle points and ★ are three maxima.

manifold of all possible incoming asymptotes. The scattering angle ϑ is the difference between the direction of the outgoing and incoming momenta.

Figure 2 is a plot of ϑ as a function of b in the interval $[-3, 3]$ for $E = 0.6$ and $\alpha = \pi$. For b outside $[-3, 3]$ the incoming projectile misses the region where the potential is essentially different from zero and there is hardly any deflection. In figure 2 we see four points where ϑ changes very rapidly as b varies. Figure 3 shows a magnification of the plot in the vicinity of such a point. One of the structures of figure 2 is resolved into several complicated substructures. In figure 4 such a substructure is magnified further and a set of even smaller substructures becomes visible, which looks very similar to the total structure shown in figure 3. Such a magnification can

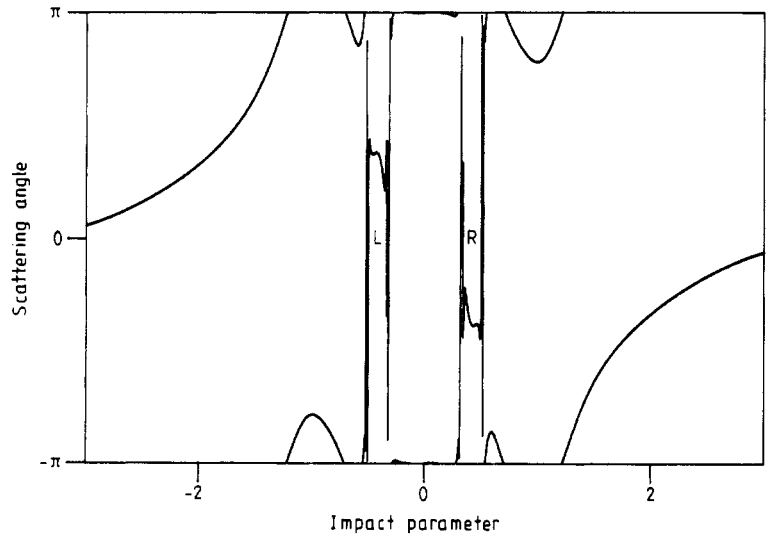

Figure 2. Scattering angle as a function of impact parameter for energy fixed at $E = 0.6$ and incoming direction fixed at $\alpha = \pi$.

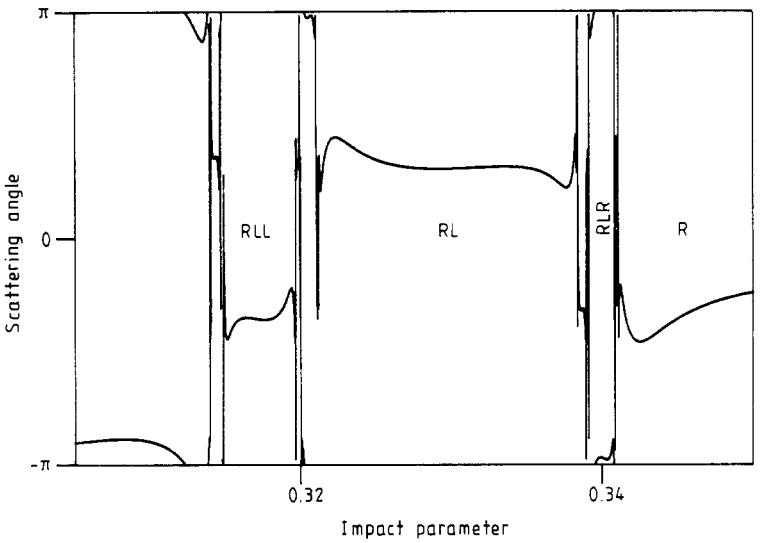

Figure 3. Magnification of figure 2.

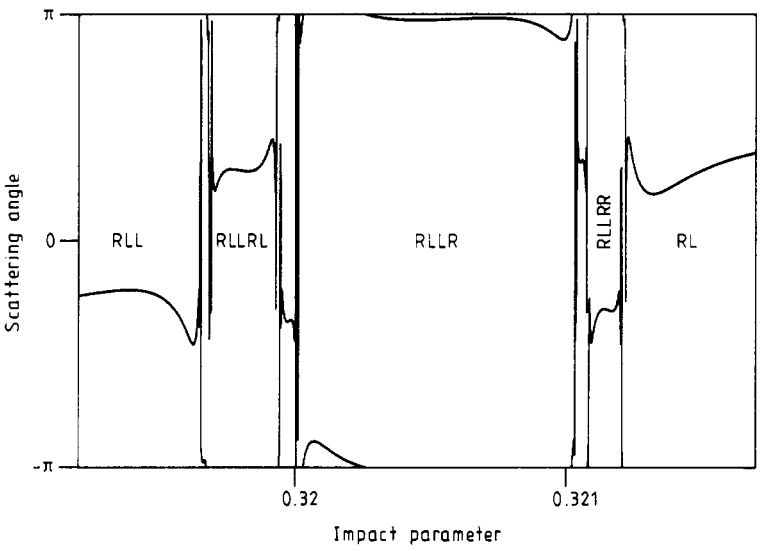

Figure 4. Magnification of figure 3.

apparently be repeated any number of times and we always obtain plots that look similar. This self-similarity of the structures under magnification is typical for Cantor sets.

In figures 2-4 we have labelled the gaps of the Cantor set by finite sequences of the letters R (standing for right) and L (standing for left). The rule for this signature is as follows: on the magnification level 1 (see figure 2) we assign the symbol L to the gap between -0.49 and -0.35 and the symbol R to the gap between 0.35 and 0.49. Under magnification new gaps appear near the ends of the intervals L and R. These gaps of level 2 are denoted by sequences of two letters. The first letter is the same as

the letter of the nearest gap of level 1. The second letter becomes L or R according to whether the gap of level 2 lies to the left or right of the nearest gap of level 1. We continue this scheme by induction. The signature for a gap of level $n+1$ consists of $n+1$ letters. The first n letters are the signature of the neighbouring gap of level n. The last letter is L or R according to whether the new gap lies to the left or right of the corresponding interval of the next lower level. The points of the Cantor set itself are labelled by infinite L/R sequences such that the symbol sequence of a singular point P is the limit of the symbols of a sequence of gaps, which converge to P. As we shall see in § 4, this labelling is only valid locally (for some interval in α and E) and cannot be continued to all values of α and E in this form.

A first indication on the origin of the observed fractal structure in the scattering singularities can be obtained by looking at some trajectories in position space. Six examples are shown in figure 5. In figure 5(a) the scattering trajectory comes in and moves along a closed ring trajectory (called Γ in the following) several times and goes off to infinity again. In figure 5(b) the trajectory comes in and starts oscillating between two potential mountains. Finally it separates from the oscillating trajectory and moves out.

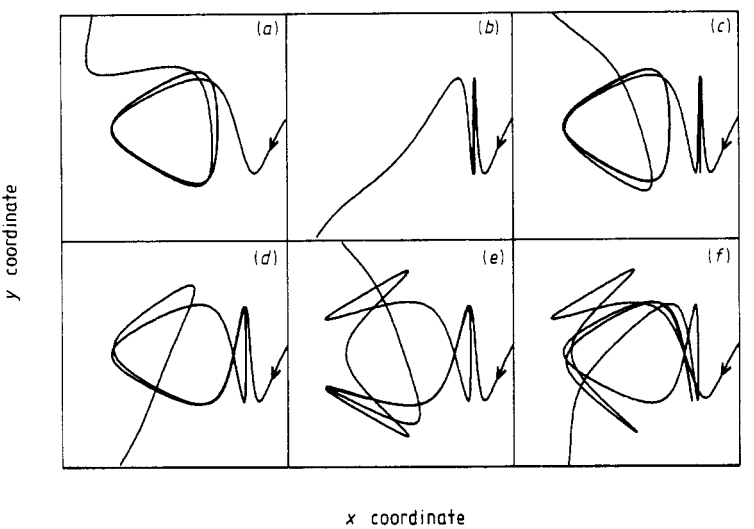

Figure 5. Six scattering trajectories in position space. The horizontal axis gives x, the vertical axis gives y. All trajectories have energy $E = 0.6$ and incoming direction $\alpha = \pi$. The impact parameters and the labels of their intervals are (a) $b = 0.501\,9226 \in$ RRLRLRLRLR; (b) $b = 0.515\,1908 \in$ RRRRRR; (c) $b = 0.515\,190\,044\,99 \in$ RRRRRRLRLR LRLR; (d) $b = 0.513\,933\,870\,501 \in$ RRRLRLLLRLRRRLR; (e) $b = 0.513\,564\,345\,433 \in$ RRRLLLRRRLLLRR; (f) $b = 0.497\,412\,858\,02 \in$ RRLLLRRLRRLRLLL.

There are similar oscillating trajectories between the other two pairs of potential mountains. In the following γ_i denotes the oscillating trajectory which passes near the saddle point P_{si}. In figure 5(c) the scattering trajectory first moves along γ_1, then switches to Γ and after a few turns along Γ goes off again. Figure 5(d) shows a scattering trajectory which switches periodically between γ_1 and Γ several times before it leaves the potential region. In figure 5(e) the middle part of the trajectory is a

sequence of pieces resembling $\frac{1}{3}\Gamma$ and successive γ_i in alternation. Figure 5(f) shows an irregular switching between pieces of the various periodic orbits.

To obtain such trajectories, it is necessary to carefully choose b from the very small intervals that carry the appropriate L/R signatures given in the figure caption. Figure 5 strongly suggests that the periodic orbits Γ, γ_1, γ_2, γ_3 and their heteroclinic and homoclinic connections have an important influence on the behaviour of the scattering trajectories.

3. Unstable periodic orbits

The properties of the priodic orbits are best investigated in Poincaré sections. Figure 6 is a plot in the (x, p_x) surface for $E = 0.6$, $y = 0$, $p_y > 0$. We have marked two fixed points A and B, their stable and unstable manifolds, two heteroclinic points C and D, and two homoclinic points E and F. In addition there are infinitely many further heteroclinic and homoclinic points not marked in figure 6. The two periodic orbits in position space corresponding to the points A and B are shown in figure 7(a). They are exactly the orbits Γ and γ_1. Figure 7(a) gives in addition the orbits γ_2 and γ_3 which do not cut the plane $y = 0$. The heteroclinic and homoclinic orbits belonging to the points C, D, E, F are shown in figures 7(f), 7(e), 7(c), 7(b), respectively.

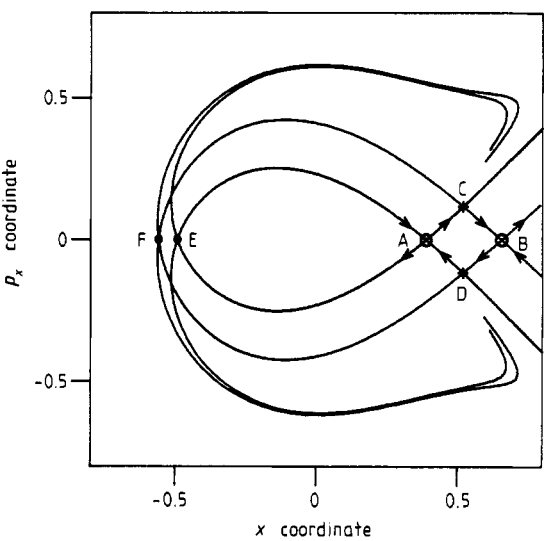

Figure 6. Poincaré plot in the surface $E = 0.6$, $y = 0$, $p_y > 0$. The horizontal axis gives x, the vertical axis gives p_x. ○ are two fixed points. The curves are parts of their stable and unstable manifolds (the complete invariant manifolds wind back and forth in an infinite number of tendrils). ★ are two heteroclinic points and ● are two homoclinic points.

The orbit Γ exists for energies between E_0 and E_M. At E_0 it emerges from the point P_0. By λ_1, λ_2 we denote the eigenvalues of the fixed point in the Poincaré section $y = 0$ belonging to Γ. At E_0 we find $\lambda_1 = \lambda_2 = 1$ because of the following reason: the potential has C_3 symmetry. Therefore the expansion of the potential around the point

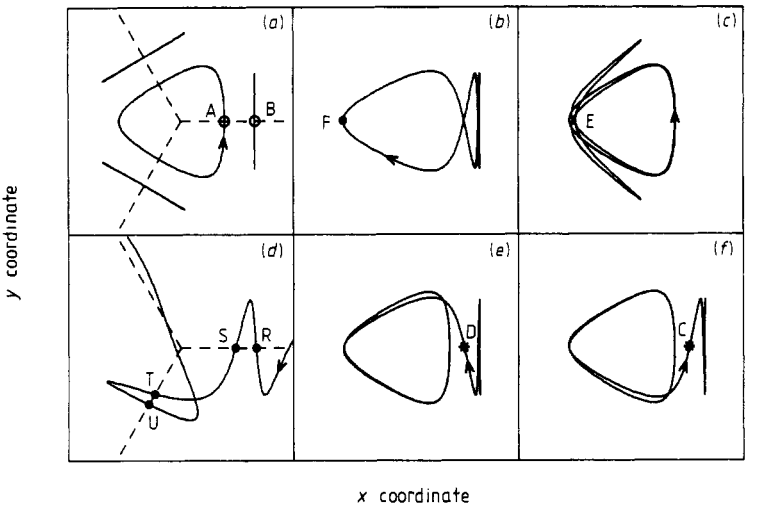

Figure 7. (*a*) The periodic orbits Γ, γ_1, γ_2, γ_3. (*b*), (*c*), (*e*), (*f*) Some homoclinic and heteroclinic orbits. A, B, C, D, E, F are the points corresponding to the points A, B, C, D, E, F in figure 6. (*d*) A typical scattering trajectory is decomposed into ingoing and outgoing parts and into oscillating and ring parts in between ($b = 0.513\,58 \in$ RRRLL). The broken lines in (*a*) and (*d*) are lines of mirror symmetry of the potential.

$P_0 = (x, y) = (0, 0)$ up to second order must be isotropic, i.e. V has an expansion $V(x, y) = E_0 + a(x^2 + y^2)/2$ plus higher-order terms where $a = 6\exp(-2)$. As long as the energy is infinitesimally above E_0 the particle starting near $(0, 0)$ moves in a two-dimensional isotropic oscillator potential. The frequencies of the two normal modes are degenerate and all trajectories are periodic and have the same recurrence time $T = 2\pi/\sqrt{a}$. Accordingly for $E \to E_0$ from above, all points near the origin in the Poincaré section become fixed points. Both eigenvalues are one for all these points. For increasing E the higher-order terms in the potential become important, the isotropy of the potential is destroyed and from the two-dimensional continuum of fixed points in the Poincaré section only the fixed point belonging to the periodic trajectory Γ survives.

With increasing energy Γ remains at first elliptic. λ_1 wanders around the upper half of the unit circle until at an energy slightly below E_s it meets the value -1. Here Γ switches from elliptic to inverse hyperbolic. With further increase of the energy λ_1 wanders along the negative real axis. At $E = 0.6$, which was used in figures 2-7, its value is $\lambda_1 \approx -83$. For $E \to E_M$ we find $\lambda_1 \to -\infty$.

The orbits γ_i exist for energies between E_s and E_M. At $E = E_s$ the orbits γ_i emerge from the points P_{si} with eigenvalues $\mu_1 \approx 47$. Again, the eigenvalues refer to the corresponding fixed points in the Poincaré sections. With increasing energy μ_1 increases too. At $E = 0.6$ $\mu_1 \approx 113$ and for $E \to E_M$ we find $\mu_1 \to \infty$. The value $\mu_1 \approx 47$ at E_s can be checked analytically. Around P_{s1} the potential can be approximated quadratically as $V = E_s - a(x - x_{s1})^2/2 + by^2/2$ plus higher-order terms where $a = 0.660\ldots$ and $b = 1.747\ldots$. Accordingly, for energies slightly above E_s, the trajectory γ_1 has the form

$$x(t) = x_{s1} \qquad y(t) = y_0 \cos(\sqrt{b}t + \varphi_0).$$

The recurrence time of the orbit is $T = 2\pi/\sqrt{b}$. Small deviations in the x direction

develop like

$$x(t) - x_{s1} = x_+ \exp(\sqrt{a}t) + x_- \exp(-\sqrt{a}t).$$

During the time T the unstable solution is amplified by the factor $\exp(2\pi\sqrt{a/b}) = 47.....$

The existence of heteroclinic and homoclinic points in figure 6 implies the existence of a hyperbolic invariant set in the Poincaré map. This in turn proves the existence of horseshoe chaos and of non-integrability of the scattering system for energies between E_s and E_M (compare the corresponding discussion in § 7 in Churchill *et al* (1979)).

The invariant set contains an infinite number of unstable periodic and an infinite number of aperiodic points, which do not go off to infinity under iteration of the Poincaré map. The three-dimensional flow in the energy surface contains the corresponding unstable periodic and aperiodic localised trajectories. All these trajectories have one branch of their stable and unstable manifold reaching out into the asymptotic region. Therefore, in the asymptotic region there is an uncountable bundle of stable manifolds of localised orbits. Transversal to the sheets of the bundle we find a Cantor set structure. Whenever the initial point of a scattering trajectory lies on one of these stable manifolds, the trajectory is attracted by a localised orbit and the scattering angle is undefined. In this way each localised orbit in the invariant hyperbolic set has an influence on the scattering behaviour similar to the influence of a circular periodic orbit in the orbiting effect in rotationally symmetric systems.

If a one-dimensional curve in $\mathcal{A}$ is selected, then this curve usually pierces the bundle of stable manifolds transversally and the points of intersection are a one-dimensional Cantor set along the curve. This gives the fractal structures seen in figures 2-4.

The set of singularities is a set of measure zero in $\mathcal{A}$. Therefore we do not hit the singularities exactly in numerical computations or in actual scattering experiments. What we see is a jump of the scattering angle when the initial condition jumps from one side of a stable manifold to the other side. Trajectories belonging to adjacent gaps of the Cantor set, having one letter more or one letter less in their L/R signature, leave the interior potential region through different saddles and therefore their scattering angles differ by approximately $\pm\frac{2}{3}\pi$. Actually between these two gaps there is an infinite number of additional smaller gaps with longer signatures. Therefore by scanning b in finer and finer steps through a tiny interval the scattering angle is seen to make more and more jumps of approximately $\pm\frac{2}{3}\pi$ each time.

Next we shall show how one can identify the regular intervals with certain classes of trajectories in position space. That is, we are looking for a rule relating any finite symbol sequence to the qualitative structure of the corresponding orbit and vice versa. As we shall see in the next section, it is not possible to assign the L/R signature globally in $\mathcal{A}$. As an example we explain how it can be given for trajectories in the rightmost singularity structure in figure 2. All these symbol sequences start with RR.

We decompose a scattering trajectory into incoming and outgoing parts and into parts in between which look qualitatively similar to one third of Γ or one half of γ_i. Let us consider, for example, the trajectory shown in figure 7(d). The part of the trajectory up to the point R is the incoming part. It is similar for all trajectories starting in impact parameter intervals having signatures beginning with RR (compare with figure 5). The next part between points R and S is qualitatively similar to $\frac{1}{2}\gamma_1$, the part between S and T has the qualitative structure of $\frac{1}{3}\Gamma$, and then comes a part similar to $\frac{1}{2}\gamma_3$ and finally the outgoing part. The symmetry lines of the potential shown as broken

lines help to make the decomposition. Now, the relation between signature and trajectory structure is the following.

By S_n we denote the symbol in position number n in the sequence. RR in position 1 and 2 gives an incoming part of the kind shown in figure 7(d). If the next symbol S_{n+1} is equal to S_n then we add an arc qualitatively similar to one of the $\frac{1}{2}\gamma_i$ (like RS in figure 7(d)). Out of the six possibilities for $\frac{1}{2}\gamma_i$ we choose that one which continues the trajectory smoothly. Likewise, if $S_{n+1} \neq S_n$, then we add an arc qualitatively similar to $\frac{1}{3}\Gamma$ with the appropriate orientation, to end up on a symmetry line again. If all symbols of the finite sequence are used up, we add an outgoing part, leaving the interior of the potential region through the pass opposite to the sector into which the trajectory has to be continued smoothly. This rule can be checked immediately for all six trajectories shown in figure 5. If any type of trajectory is wanted, we decompose it into Γ and γ parts, construct the corresponding L/R signature and know in which b interval the trajectory has to start.

For trajectories belonging to b intervals, whose symbol sequence does not start with RR, similar rules can be given with some modifications for symbols in the first three positions. There are no global rules for the connection between gaps in the Cantor set and symbol sequences and the trajectory structure, because different gaps in the one-dimensional Cantor set can be connected without crossing the Cantor set itself by changing α and/or E in addition to changing b. Such multiparameter changes affect the front parts of the trajectories with corresponding additions or deletions of symbols in the signature.

The value of λ_1 and μ_1 can be used to give approximately the scaling law of the Cantor set shown in figures 2-4. Adding L or R to the signature of an interval corresponds to adding $\frac{1}{3}\Gamma$ or $\frac{1}{2}\gamma_i$ to the interior part of the orbit. In order to stay for an additional third or half revolution on the unstable periodic orbit Γ or γ the precision of the initial impact parameter must be increased by a factor $|\lambda_1|^{1/3}$ or $\mu_1^{1/2}$, respectively. These numbers also give the relation between the lengths of intervals having one digit more or less in their signatures. For example, in figure 4 we measure

$$\text{length(RLLRL)/length(RLLR)} \approx 0.21\ldots \approx |\lambda_1(E=0.6)|^{-1/3}$$

$$\text{length(RLLRR)/length(RLLR)} \approx 0.10\ldots \approx (\mu_1(E=0.6))^{-1/2}.$$

4. Global structure of the scattering singularities

An incoming scattering asymptote is labelled by the three quantities E, α, b. Therefore $\mathscr{A}$ is a three-dimensional manifold. Let $\mathscr{S}$ be the subset of $\mathscr{A}$, which leads to singularities of the scattering angle, i.e. $\mathscr{S}$ is the set of incoming asymptotes which lie on the stable manifold of localised orbits. In this section we give a graphical representation of this set. Figures 8 and 9 show the intersection of $\mathscr{S}$ with different planes of $\mathscr{A}$. In figure 8 we see the singularities emerging from the saddle points at energy E_s and disappearing in the mountain tops at energy E_M. For energies outside the interval $[E_s, E_M]$ there are no invariant manifolds of unstable periodic orbits reaching out into the asymptotic region. Accordingly there are no singularities of the scattering outside $[E_s, E_M]$. Figure 9 gives several slices through $\mathscr{S}$ in (α, b) planes with $E =$ constant. It clearly shows how the gaps in the one-dimensional Cantor sets along lines $\alpha =$ constant are connected in higher dimensions. Accordingly, the labelling of the gaps of the one-dimensional

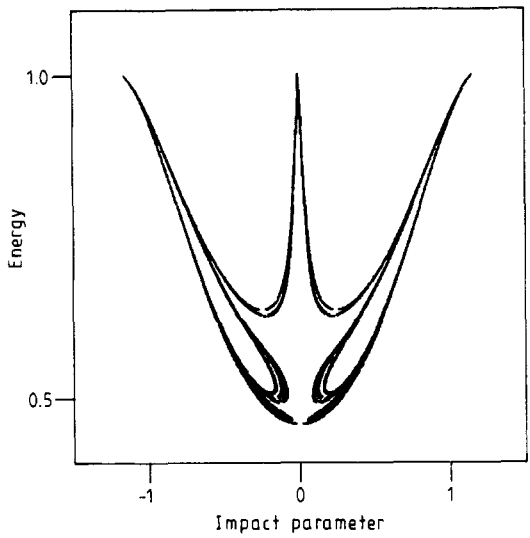

Figure 8. Cantor set of singularities of the scattering angle in the E/b plane for $\alpha = \pi$. The horizontal axis gives b, the vertical axis E.

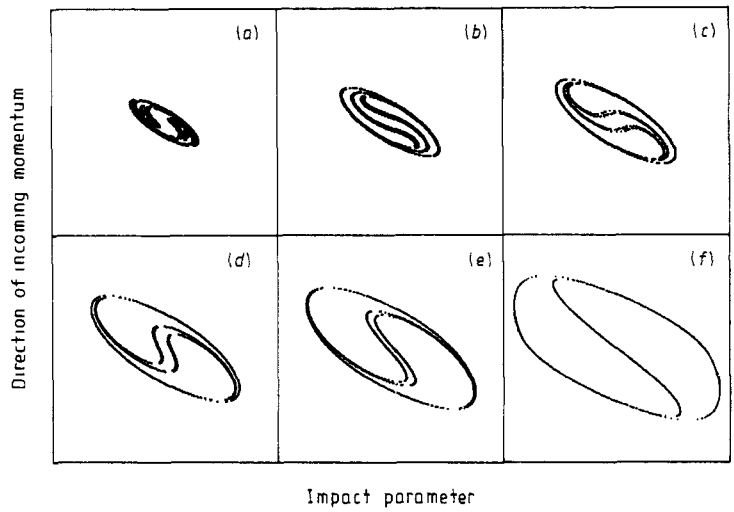

Figure 9. Cantor set of singularities of the scattering angle in the α/b plane for several values of $E = 0.5$ (a), 0.55 (b), 0.6 (c), 0.7 (d), 0.8 (e), 1.0 (f). The horizontal axis gives b, the vertical axis α in the interval $[\frac{2}{3}\pi, \frac{4}{3}\pi]$. It looks the same in intervals shifted by $\pm\frac{2}{3}\pi$.

Cantor set by symbol sequences, as done in § 2, is only valid along particular one-dimensional lines. In this sense any rule for the connection between L/R signatures and the qualitative structure of the trajectories is only valid locally.

5. Conclusions

This paper illustrates how a Hamiltonian flow can become chaotic on non-compact energy surfaces, i.e. in scattering systems. The chaos shows up in Cantor sets of

singularities of the scattering angle as a function of the initial conditions. The proof of non-integrability of the Henon-Heiles system given by Churchill *et al* (1979) can be carried over exactly to our system. Thereby it becomes evident that no additional global conserved quantity exists on energy surfaces with energy between E_S and E_M.

Similar chaotic behaviour of scattering systems should be expected in all potentials having several relative maxima and some saddle points in between, such that there are several unstable periodic orbits having heteroclinic and homoclinic connections. We have checked some other potential models and have found fractal structures in the scattering singularities in those systems, which fulfil the above-mentioned criteria.

Can the singularities have some influence on a real scattering experiment? In an actual scattering experiment E and α are held fixed and a broad stream of particles, having different values of b, is sent towards the target. The number of particles going off in various final directions is monitored. Accordingly, the differential cross section contains a summation over all contributing impact parameters. By this summation the effects of singularities may be smeared out.

If real experiments are done on microscopic systems, e.g. scattering of atoms or electrons from triangular or triatomic molecules, then quantum effects must be taken into account. They have the tendency to wash out effects of classical singularities further. We would expect to see a superposition of an infinite number of structures as they appear in orbiting scattering in rotationally symmetric systems. For a discussion of the connection between classical and quantum orbiting scattering see Korsch and Thylwe (1983). We consider it to be worth investigating whether any visible effect of the singularities is left over after this averaging.

Acknowledgments

We thank Professor P H Richter and Dr B Eckhardt for stimulating discussions. This work was supported financially by Stiftung Volkswagenwerk.

References

Churchill R C, Pecelli G and Rod D L 1979 *Stochastic Behaviour in Classical and Quantum Hamiltonian Systems* (*Lecture Notes in Physics* **93**) ed G Casati and J Ford (Berlin: Springer) pp 76-136

Eckhardt B and Aref H 1987 in preparation

Eckhardt B and Jung C 1986 *J. Phys. A: Math. Gen.* **19** L829-33

Gottdiener L 1975 *Mol. Phys.* **29** 1585-95

Henon M and Heiles C 1964 *Astron. J.* **69** 73-9

Korsch H J and Thylwe K E 1983 *J. Phys. B: At. Mol. Phys.* **16** 793-815

Newton R G 1982 *Scattering Theory of Waves and Particles* (Berlin: Springer)

Noid D W, Gray S K and Rice S A 1986 *J. Chem. Phys.* **84** 2649-52

Petit J M and Henon M 1986 *Icarus* **66** 536-55